Multi-parametric investigations on the effects of vascular disrupting agents based on a platform of chorioallantoic membrane of chick embryos

Lei Chen[1]^, Mingpei Wang[2], Yuanbo Feng[1], Lingjie Gao[1], Jie Yu[1], Lei Geng[3], Yiyang Xie[4], Walter Coudyzer[5], Yue Li[4], Yicheng Ni[6]

[1]KU Leuven, Theragnostic Laboratory, Campus Gasthuisberg, Leuven, Belgium; [2]Faculty of Innovation Engineering, Macau University of Science and Technology, Macau, China; [3]School of Life Science, TianGong University, Tianjin, China; [4]Shanghai Key Laboratory of Molecular Imaging, Shanghai University of Medicine and Health Sciences, Shanghai, China; [5]Department of Radiology, University Hospitals Leuven, KU Leuven, Leuven, Belgium; [6]Department of Radiology, Zhongda Hospital, Southeast University, Nanjing, China

Contributions: (I) Conception and design: L Chen, Y Ni, Y Li; (II) Administrative support: L Chen, Y Feng, J Yu; (III) Provision of study materials or patients: L Chen, Y Feng; (IV) Collection and assembly of data: L Chen, M Wang, L Gao, J Yu, L Geng; (V) Data analysis and interpretation: L Chen, M Wang, L Gao, J Yu, L Geng; (VI) Manuscript writing: All authors; (VII) Final approval of manuscript: All authors.

Correspondence to: Yicheng Ni, MD, PhD. Department of Radiology, Zhongda Hospital, Southeast University, Dingjiaqiao No. 87, Nanjing 210009, China. Email: yicheng.ni@oncocidia.com; Yue Li, PhD. Shanghai Key Laboratory of Molecular Imaging, Shanghai University of Medicine and Health Sciences, Zhouzhu Road No. 279, Shanghai 201318, China. Email: liy_16@sumhs.edu.cn.

Background: Vascular disrupting agents (VDAs) are known to specifically target preexisting tumoural vasculature. However, systemic side effects as safety or toxicity issues have been reported from clinical trials, which call for further preclinical investigations. The purpose is to gain insights into their non-specific off-targeting effects on normal vasculature and provide clues for exploring underlying molecular mechanisms.

Methods: Based on a recently introduced platform consisting laser speckle contrast imaging (LSCI), chick embryo chorioallantoic membrane (CAM), and assisted deep learning techniques, for evaluation of vasoactive medicines, hemodynamics on embryonic day 12 under constant intravascular infusion of two VDAs were qualitatively observed and quantitatively measured in real time for 30 min. Blood perfusion, vessel diameter, vessel density, and vessel total length were further analyzed and compared between blank control and medicines dose groups by using multi-factor analysis of variance (ANOVA) analysis with factorial interactions. Conventional histopathology and fluorescent immunohistochemistry (FIHC) assays for endothelial cytoskeleton including ß-tubulin and F-actin were qualitatively demonstrated, quantitatively analyzed and further correlated with hemodynamic and vascular parameters.

Results: The normal vasculature was systemically negatively affected by VDAs with statistical significance (P<0.0001), as evidenced by four positively correlated parameters, which can explain the side-effects observed among clinical patients. Such effects appeared to be dose dependent (P<0.0001). FIHC assays qualitatively and quantitatively verified the results and exposed molecular mechanisms.

Conclusions: LSCI-CAM platform combining with deep learning technique proves useful in preclinical evaluations of vasoactive medications. Such new evidences provide new reference to clinical practice.

Keywords: Chorioallantoic membrane (CAM); laser speckle contrast imaging (LSCI); vascular disrupting agents (VDAs); fluorescent immunohistochemistry (FIHC); endothelial cytoskeleton

---

^ ORCID: 0000-0002-8620-6186.

Introduction

As a major branch of vascular-targeting therapies (VTTs), vascular disrupting agents (VDAs) have been ardently explored over the last two decades for potential anticancer purpose (1,2). According to the definition, VDAs specifically target existent tumoural vasculature by acting on, and exploiting the intrinsic defect of, their endothelial cells, and consequently cause vascular shutdown, blood flow stoppage and pervasive necrosis in the tumor interior that usually resists to conventional chemotherapy and radiation therapy (3-5). Noticeable specificity is that VDAs can leave normal tissue relatively intact (6) or affect little on non-malignant tissues (3), revealing a mild safety profile among tested patients.

Based on preclinical and clinical studies, a viable rim always remains in the tumors after intravenous (IV) administration of VDAs, presumably because it derives nutrients from adjacent normal blood vessels (6,7). Therefore, to overcome such incomplete anticancer efficacy, multiple doses of VDAs are often combined with other modalities such as chemotherapy (8-10), anti-angiogenic agents (AAs) (11,12), AAs and chemotherapy (13) and radiation therapy (14). But the outcomes of phase II-III clinical trials on VDAs with both monotherapy and combinational therapy are still unsatisfactory due to rapid tumor regrowth and poor ultimate drug efficacy resulting from viable tumor residues at the periphery, which impeded the authority approvals on oncological applications of VDAs (7). To tackle such bottleneck problems of tumor residue and cancer relapse common to all VDAs, a dual targeting pan-anticancer theragnostic strategy called OncoCiDia has been attempted, in which a single dose of VDA is first used to create massive tumor necrosis that serves as the target for a secondary single dose of a radio-iodinated necrosis-avid compound hypericin on the next day to exert local persistent irradiation-cleansing of the remaining cancer cells due to I-131's 8-days decaying half-life and emission of high energy betta particles. The co-emitted gamma rays can also facilitate nuclear imaging of the cancer under treatment, hence a true theragnostic property of OncoCiDia (15).

Meanwhile, a number of safety issues have been reported from clinical trials with VDAs (16). Besides other adverse effects including dyspnea, tumour pain, abdominal pain, neurotoxicity, headache, nausea and vomiting (5,16,17), cardiovascular toxicities are prominent with hypertension as the most common one, followed by QTc prolongation, tachycardia and bradycardia, myocardial infarction, and atrial fibrillation (17). These systemic side effects or off-target toxicities are characterized by acute, transient, noncumulative and reversible natures (16), but are rather difficult to explain by VDAs' specificity on tumoural vasculature, with a few hypotheses being proposed. For instance, VDAs can impact on non-malignant tissues (18) either directly on the healthy organs/tissues or indirectly by the cytokines released when VDAs act on tumor-related blood vessels (16). Hypertension induced by VDAs is a compensatory response to an increase in peripheral resistance (18), and VDAs may influence blood pressure by activating the angiotensin-renin system (19). These uncertainties call for further laboratory research.

The purpose of this study is to gain more insights into the non-specific effects of VDAs on normal vasculature and provide clues for exploring underlying molecular mechanisms, in order to substantiate those hypotheses and propose possible directions for VDA research.

The chick embryo with chorioallantoic membrane (CAM) possesses all necessary organs and circulatory system of vertebrates, as complete living form (4) and the CAM has been proved as suitable *in vivo* model to study numerous anti-cancer therapies (20-22), toxicant vascular effects (23), and molecular mechanisms (24,25). A laser speckle contrast imaging (LSCI)-CAM platform for evaluation of vasoactive medications has been introduced recently (26), which could be an ideal means to study VDAs' non-specific effects on normal vasculature.

We designed and performed the present experiment to answer the following questions. (I) Is it feasible to do VDA studies on normal vasculature at a recently established LSCI-CAM platform? (II) Are multiple parameters such as blood perfusion, vascular diameter, density and length affected by VDAs? (III) Whether such parameters can be recorded and quantified by the platform? (IV) Can we gain any molecular insight into the mechanisms of VDAs particularly with fluorescent immunohistochemistry (FIHC)? And (V) to what extent can the results from this
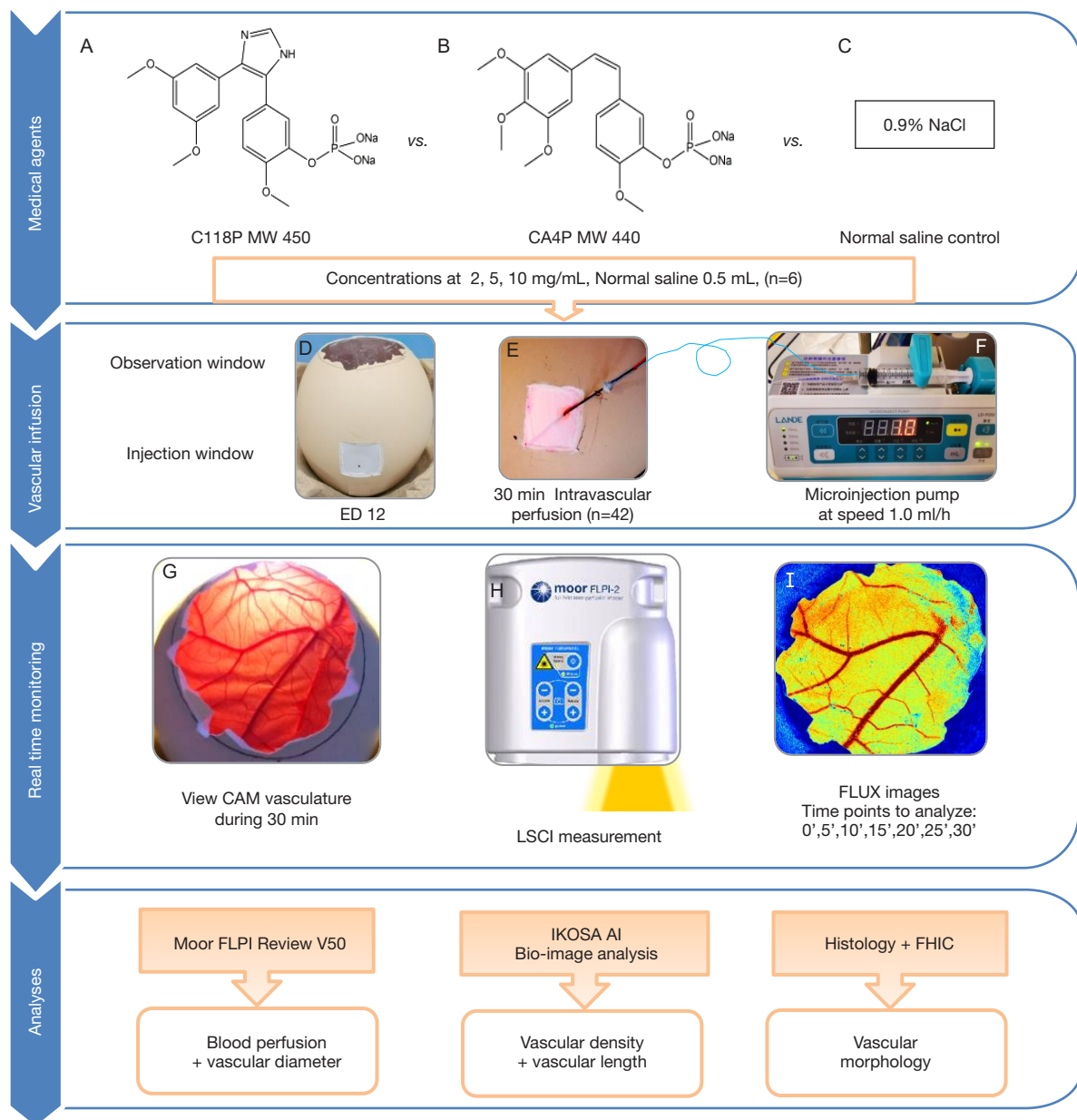
Figure 1 Flow chart of experimental protocol. C118P, C118 phosphate; CA4P, combretastatin A4-phosphate; CAM, chorioallantoic membrane; LSCI, laser speckle contrast imaging; FLPI, full-field laser perfusion imager; FIHC, fluorescent immunohistochemistry.

study on CAM explain clinical pharmacologic and adverse effects of VDAs?

Methods

Ethical approval was waived by the Institutional Ethics Committee of KU Leuven since chick embryos are not considered animals before ED18, in compliance with The European Parliament and the European Council Directive 2010/63/EU (24,27). The present experimental study on chick embryos was executed according to the protocol as illustrated in *Figure 1*.

Studied agents

C118 phosphate (C118P) as a new CA4P analogue of VDAs

was supplied by Nanjing Sanhome Pharmaceutical Co. Ltd (Nanjing, China) (*Figure 1A*). Combretastatin A4-phosphate (CA4P) as a benchmark VDA was purchased from Shanghai Yuanye Biotech Co. Ltd (Shanghai, China) (*Figure 1B*). Sterile 0.9% normal saline (B. Braun, Melsungen, Germany) was used as a vehicle control agent (*Figure 1C*).

Chick embryo incubation and preparation for catheterization

Freshly laid fertilized chicken eggs (Xinyang species) were provided by Shanghai Poultry Breeding Co. Ltd (Shanghai, China). On embryonic day (ED) 1, the eggs were transferred into a digital incubator (Rcom MARU MAX, Korea). The blunt side of every embryonic egg was facing upward and fixed within the holding tray and maintain at 37.5 ℃ and 65% humidity during incubation process. The trays changed ±45° angle automatically every hour for balanced development of embryo. On ED 12 as an optimal moment (26), when CAM vessels have the most suitable status (size, maturity, richness, blood flow and locations) to be monitored and analyzed responding to different vasoactive medications, embryos were taken out from incubator to the ambient laboratory consecutively for the in ovo experiment.

A circular observation window about 2.0 cm in diameter was opened on the egg shell along the edge of the air cell (*Figure 1D*), and a square injection window about 1.0 cm^2 in size on the lateral shell was opened carefully to expose an underneath major CAM blood vessel (*Figure 1E*) as described in details previously (26).

A custom-made fine needle catheter of 30 Gauge was produced and connected with the micro-injection pump through a silicon micro-tube (*Figure 1E,1F*). After the CAM blood vessel was punctured and catheterized by the tiny needle at the injection window, intravascular drug administration was driven by the micro-injection pump, while the rest of CAM still remained intact (26,28) (*Figure 1D-1G*).

Equipment hardware and software

An LSCI centered platform included one full-field laser perfusion imager (FLPI) from Moor Instruments (www.moorclinical.com, Devon, UK) (*Figure 1H*), a wire-connected desktop computer and catheter-infusion-pump unit. An electric blanket was put underneath the egg holder to simulate incubator temperature about 37.5 ℃ and to avoid cold stress of embryo during the experiment. Imaging

settings were configured as: camera auto focus, auto gain, 180° rotation and low-speed/high-resolution; default 20 ms integration time; 250 images at a 10-second interval as temporal filter to reconstruct one effective frame for analysis; thus 30 min measurement could generate 180 integrated frames. The position and system parameters were kept constant during each entire experiment (26).

Regarding the working mechanism of LSCI technique, the FLPI device projects laser light on the tissue surface and generates a random interference, which yields different contrasts, named as laser speckle patterns sensitive to blood flow velocity that is coded into a contrast intensity map. The flowing red blood cells in a blood vessel decreases the contrast, so the blood flows with high speed reveal low contrast regions and conversely low blood flow speed appears as high contrast (29-32).

Speckle contrast Flux images generated from LSCI-CAM platform can be processed by the connected PC with the software Moor FLPI Review V5.0 (Moor Instruments Ltd., UK) to display and analyze those images (*Figure 1I*). In addition, ImageJ Fiji Software (https://imagej.nih.gov/ij/index.html) was used to measure vessel diameter (26). The vessel diameter is an important parameter to represent chick vascular status and network, as described in (33).

To explore the above Flux images for more extended parametric analyses, this study also adopted a commercial deep learning aided IKOSA® platform (www.ikosa.ai) produced by KML Vision GmbH (www.kmlvision.com, Graz, Austria), which is dedicated for bio-image data management and automated analysis in the field of the pharmaceutical and medical sciences. An existing IKOSA Prisma deep learning-based algorithm, CAM Assay-V 3.0.0, was kindly provided by the company and implemented in this research.

Experimental protocol

According to the maximum tolerated doses (MTDs) derived from animal studies and clinical trial experiences (34), two VDAs were dissolved with 0.9% saline into three concentrations: 10, 5 and 2 mg/mL, respectively. As shown in *Figure 1*, on the predetermined optimal ED 12 (26), altogether 42 chick eggs were randomly divided into 6 treatment groups for receiving intra-vascular administrations of the above 3 concentrations of either C118P or CA4P, and a vehicle control group receiving 0.9% saline, respectively (n=6, each).

Through injection window, 0.5 mL of a VDA solution was infused into a CAM surface blood vessel for 30 min, via

a microinjection pump at a speed of 1 mL/h (approximately 15 µL/min). Multiparametric measurements were performed simultaneously on the CAM-LSCI platform for real time monitoring of vascular and hemodynamic changes at an analytical interval of every 5 min (*Figure 1*). Conventional monitoring parameters include blood perfusion (Flux) and vascular diameter (26); in addition IKOSA deep learning platform contributed two more parameters of vascular density and vascular total length. Histology of HE staining and FIHC analysis were carried out to explore microscopic molecular insights.

Monitoring and data acquisition

Intravascular infusion, LSCI real time monitoring and data acquisition were simultaneously conducted during 30 min for this in ovo experiment in the laboratory environment at temperature about 22–23 ℃.

The head of FLPI device was positioned 25 cm upright above observation window of the egg embryo. The correct positioning was facilitated by targeting beam (red laser) to the field of interest, which can be controlled by PC software of "zoom" function. With this LSCI-CAM platform, the CAM hemodynamics and vasculature could be real time scanned efficiently for dynamically monitoring and capturing the alterations of blood perfusion and microcirculation during the pharmacological interventions with VDAs, and recorded by the PC for analyses by the software. Based on generated real-time 2D images (Flux), regions of interests (ROIs) are determined by drawing a 1.0 mm^2 circle on a major vessel trunk in the observation window, as previously optimized (26). Mean perfusion unit values (PU) during 30 min were reported and analyzed by the software based on ROIs of all embryos of different treatment groups and thereby all real-time perfusion results were exported into one graph as a function of time for further statistical analyses.

The diameter measurements were designated at junction point of major vessels near its branch, facilitating the fixation of the position. The diameters of the same-positioned vasculature on 2D image of individual CAMs were quantified using MoorFLPI-2 review software V5.0 with the accuracy of a millimeter scale and those images were transferred to ImageJ (Fiji software) for distance measurement at a micrometer level.

Two parameters of vascular density ($\frac{\text{vessel total area}}{\text{ROI area}}$) and vascular total length were elaborated by using IKOSA deep learning system. First, Flux images generated from LSCI-CAM platform were converted into grayscale ones, and then uploaded into the image library of IKOSA deep learning platform. Every selected image was encircled in a 2 cm^2 circle from the whole image as a ROI. Analytical resolution of images could reach 10 µm/Pixel. The results of relevant parameters for the quantification of blood vessels on CAM assays were automatically reported following IKOSA deep learning algorithm analyses. The parameters selected for this study were defined by comparing phenotypic characteristics of normal vessels or tumoral vessels (5) as well as the capacities of the applied LSCI-CAM platform.

Histology and cytoskeleton FIHC analyses

One piece of major vessel at observation window was excised into a centrifugal tube, and undertaken shock cooling by liquid nitrogen, followed by deep frozen storage at –80 ℃. The specimens were sectioned at 8 µm by a cryotome, and stained with hematoxylin-eosin (HE) staining for histological analysis. The observations and documentation were executed under a digital section scanner NanoZoomer S210 with the software NDP view2 (Hamamatsu, Japan).

For FIHC, β-tubulin and F-actin (filamentous actin) are two predominant proteins within endothelial cytoskeleton of blood vessels, which are identified in this immunofluorescence double-staining protocol as detailed below.

Slides of frozen sections at 8µm were kept at room temperature to defrost for of 30 min, followed by (I) three times washing for 5 min with phosphate buffered saline (PBS); (II) treatment in PBS containing 0.1% Triton X-100 (PBS-T) and three times of PBS washing for 5 min; (III) specimens being blocked with goat serum for 30min before incubation with antibodies; (IV) specimens being incubated with the first antibody for anti-β-tubulin (ABCAM, ab179513) in 1:50 overnight at 4 ℃ in wet box and three times of PBS washing for 5 min; (V) using a FITC (fluorescein isothiocyanate)-conjugated goat anti-rabbit (ABCAM, ab150077) kit in 1:100 as a secondary antibody for anti-β-tubulin for 30 min under dark incubation at room temperature and three times of PBS washing for 5 min; (VI) using Phalloidin iFluor 555 (40737ES75) at 1:100 in PBS-T for 60 min under dark incubation at room temperature to label, identify and visualize spectrum red F-actin followed by three times of PBS washing for 5 min; (VII) specimens being washed and embedded with 4',6-diamidino-2-phenylindole (DAPI, Sigma, D9542) to stain nuclei; and (VIII) sealing slides by anti-fluorescence

quenching agent. Finally, immunofluorescence images were obtained by fluorescence scanner PANNORAMIC MIDI II (3D Histech, Hungary), equipped with three filter sets for FITC (spGreen), Phalloidin (spOrange), and DAPI (spBlue). Mean fluorescent intensity of β-tubulin and F-actin at each immunofluorescence images were determined by image analysis software VISIOPHARM 2022.07 (Visiopharm, Denmark).

Data process and statistical analysis

All parameters including blood perfusion, vessel diameter, vascular density and vascular length were expressed as the mean ± standard error of the mean (SEM). Statistical analyses were performed by using SPSS (for Windows Version 23, IBM, Chicago, IL, USA) and MATLAB (R2016b, MathWorks Inc., NATICK, MA, USA). In all experiments of this research, analytical time points were designed for every 5 min interval starting from 0 min until 30 min. Because of the variations among individual eggs, relative values or ratios of the multiple parameters against the initial values on time point zero were adopted for quantifications and comparisons of vascular parameters, which conform to the published literature (26,35). The ratio greater than 1.0 means an increase in parameters, whereas the ratio smaller than 1.0 indicates a decrease in the parameters. The higher fluctuation of increase or decreases of the ratio, the more significant were the true value changes. Such relative values proved more realistic for the comparison and interpretation of the data and results. All multivariate analyses were carried out by using the multi-factor analysis of variance (ANOVA) with factorial interactions. Linear regression was applied for correlation analyses of every two parameters, in which Pearson correlation coefficients were obtained. The values of $P<0.05$ were considered statistically significant (*Figure 1J*).

Results

General aspects

All chick embryos (n=42) kept alive well during the incubation period until ED12 when the experiment was executed. The injection window on the eggshell uniformly in size of 1 cm^2 could cover a pre-captured major lateral blood vessel for catheterization and pump infusion of a VDA or normal saline, whereas the observation window opened at the air-chamber averaging 2.6±0.23 cm (mean ± SEM) in diameter could ensure imaging acquisitions with LSCI during 30 min, followed by cracking the egg for tissue sampling (*Figure 1*). ED12 proved to be an optimal date for VDAs evaluation on CAM as suggested earlier (26).

Functional & morphological alterations on CAM vasculature detected by LSCI

Qualitative observations

From the series of images generated from LSCI-CAM platform (*Figure 2*) and subsequent IKOSA deep leaning platform (*Figure 3*), a trend of obvious alterations on the four parameters could be discerned. Blood perfusion as a functional parameter was demonstrated by the images acquired at serial time points during infusion of a VDA of different concentrations, taking those with C118P as examples (*Figure 2*). From *Figure 2*, the control group hardly displayed any changes throughout 30 min administration of normal saline. Whereas, with a VDA (C118P or CA4P), blood perfusion initially enhanced during the first 10–15 min at levels proportional to administered drug volumes, but decayed with time until the end of treatments. From the gradually altered images, overall evolutions could be observed at all categories of blood vessels. The coexisting red shadows besides blood vessels on CAM Flux images (*Figure 2*) were caused presumably by the underneath embryo structures (for instance vasculature or other capillary networks on the vitelline membrane) with ample blood perfusion.

The bifurcation point of major vessels was always selected for the measurement of vascular diameters (*Figure 2*), which displayed a similar trend as that with blood perfusion, i.e. constant with saline control group but decreasing during 30-min VDA treatments in a dose-dependent manner. The transient slight diameter increase around 10–15 min could be attributed to the volume effect of infused liquid, which was overcome by the later VDA pharmacologic effect.

The density and total length of vessels as two additional parameters determined by IKOSA deep learning platform are discerned in *Figure 3*, taking those with CA4P as examples for interpretation. During the first 10–15 min, both the density and length of CAM blood vessels were visually increasing, which then followed by attenuation or diminishing until the end of VDA administration at 30 min, findings similar to Flux and diameter changes in *Figure 2*.

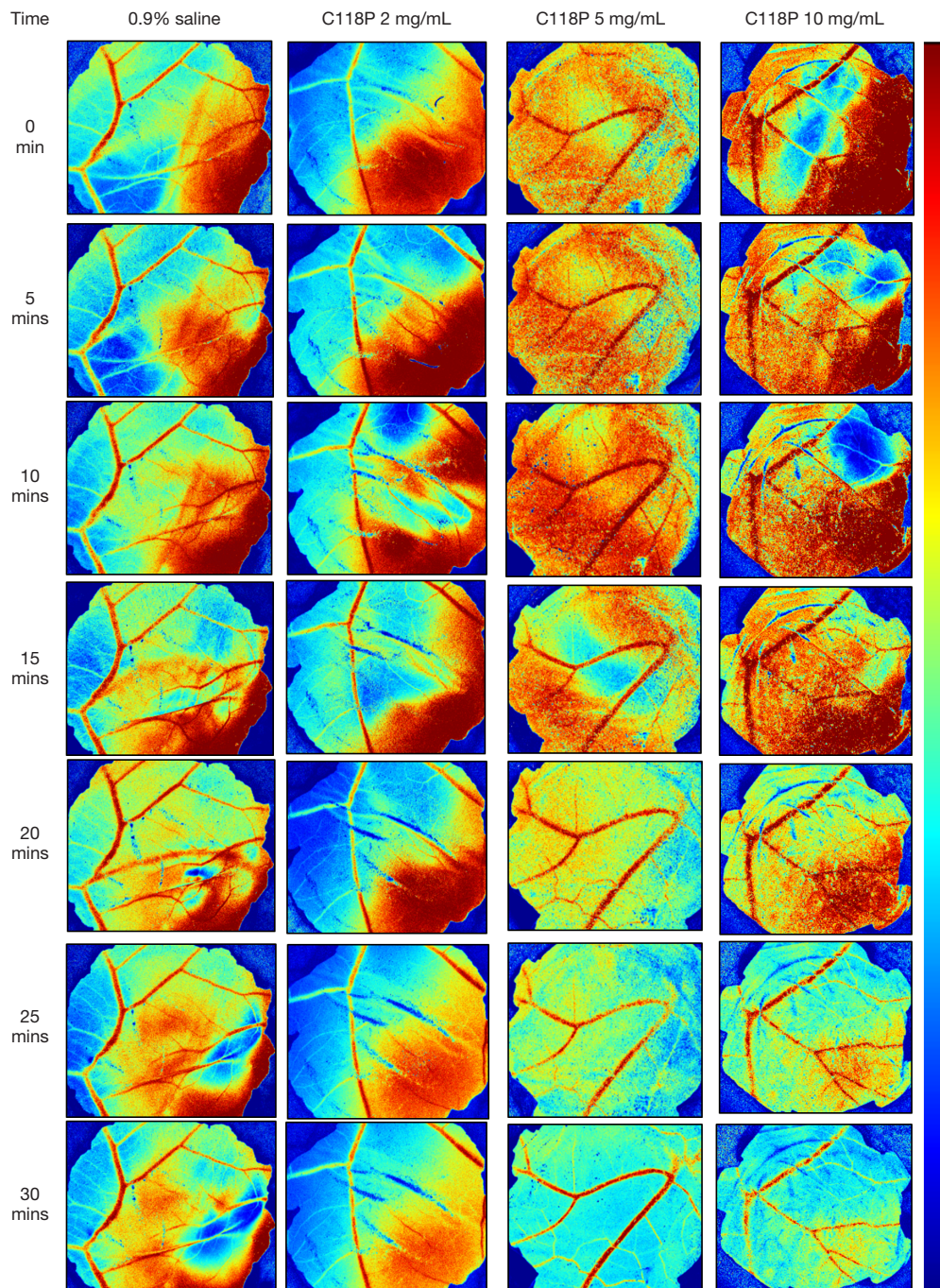By contrast, control group did not show any pharmacologic effect on vascular density and total length

Figure 2 FLPI captured Flux images of blood perfusion in CAM sequentially generated by the LSCI-CAM platform. Horizontal line lists 0.9% saline control, 2 mg/mL, 5 mg/mL, 10 mg/mL of C118P; vertical line lists successive analytical time points; color bar at right side is PU indicator. FLPI, full-field laser perfusion imager; CAM, chorioallantoic membrane; LSCI, laser speckle contrast imaging; PU, perfusion unit values.
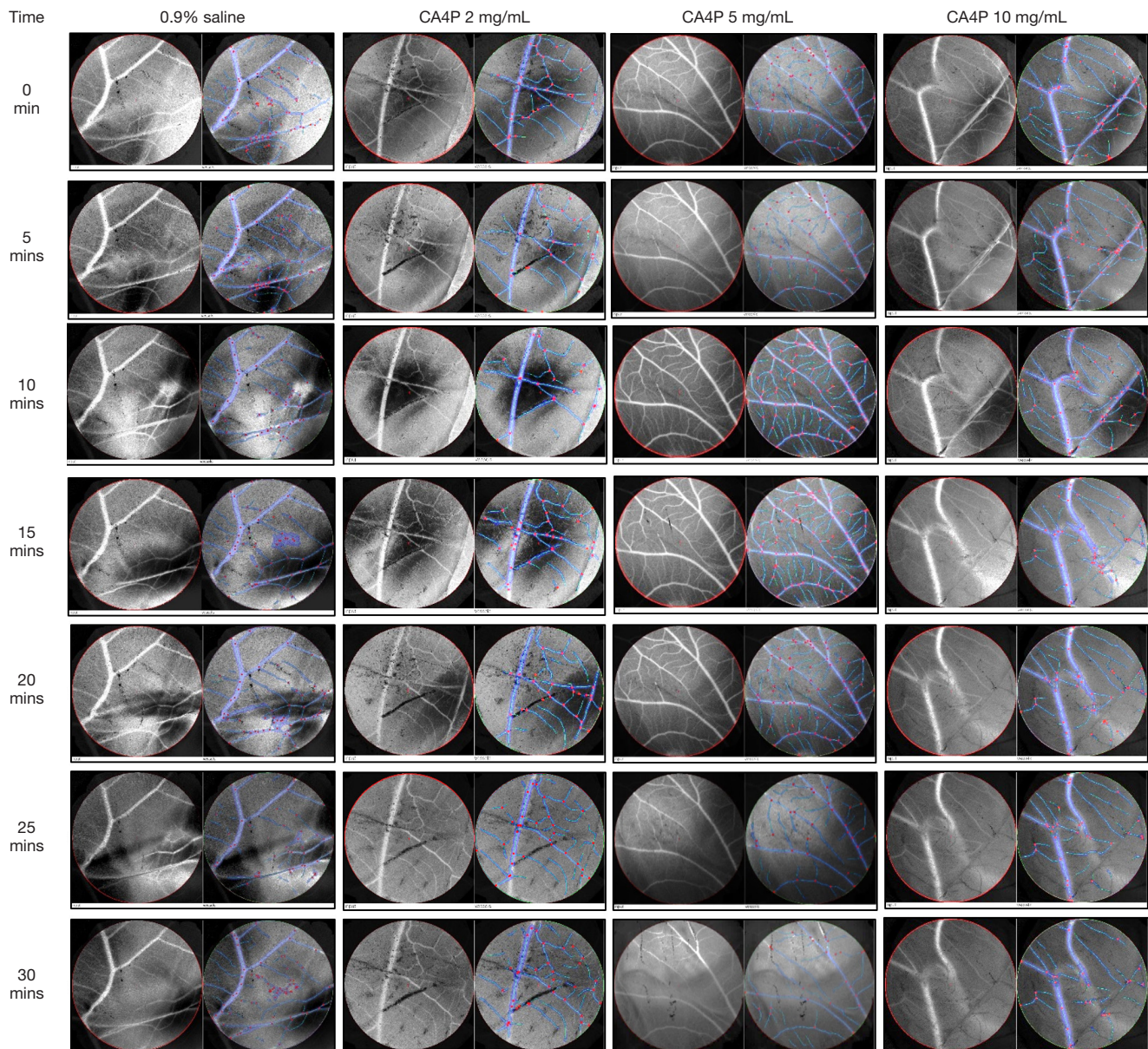
Figure 3 CAM images analyses using the IKOSA Prisma deep learning model, CAM Assay-V 3.0.0. Resulting images were sequentially generated and displayed. Horizontal line lists 0.9% saline control, 2, 5, 10 mg/mL of CA4P; vertical line lists successive analytical time points. Each item includes two ROI-delineating images, left one being input image in grayscale from LSCI-CAM platform, and right one being interpretative results of blood vessels by IKOSA platform. CAM, chorioallantoic membrane; ROI, region of interest; LSCI, laser speckle contrast imaging.

but with only slight volume effect during normal saline infusion.

Quantitative measurements
LSCI-CAM and IKOSA deep learning platforms provided quantitative analytical results. Blood perfusion

(*Figure 4A*) was influenced by VDAs during the administration. Among both VDAs, 10 mg/mL caused approximately 40% reduction of blood perfusion; 5 mg/mL induced approximately 20–25% reduction; but 2 mg/mL only yielded approximately 5–8% reduction. For this functional parameter, there is no statistically significant
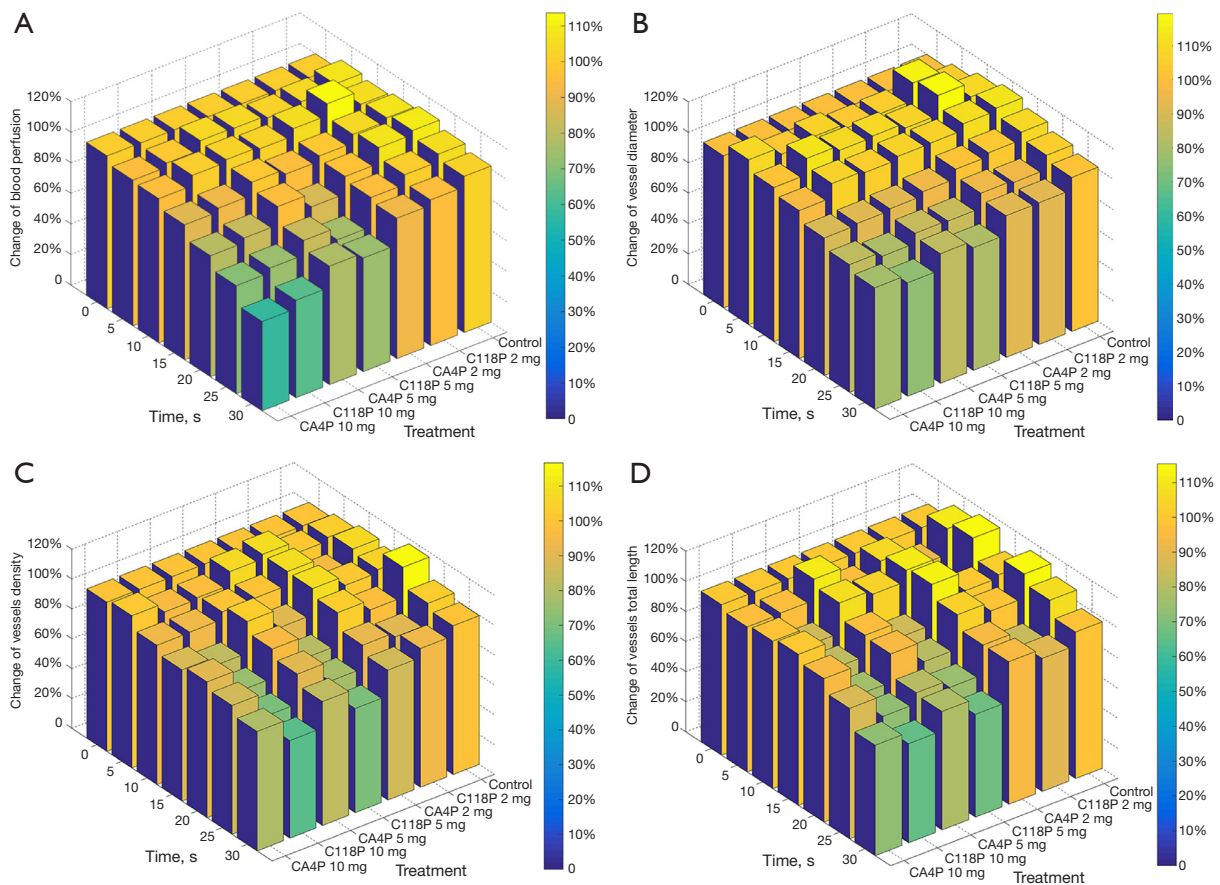
Figure 4 Three-dimensional plots of relative values from multiple parameters comparing saline control group with two VDAs of 3 doses each. (A) Blood perfusion; (B) vessel diameter; (C) vessel density; (D) vessel total length. Color bar at right side is the heatmap indicator. VDAs, vascular-disrupting agents.

difference between CA4P and C118P on their CAM perfusion effects.

Vessel diameter (*Figure 4B*) altered at a smaller scale relative to that with the blood perfusion. Among two VDAs, 10, 5 and 2 mg/mL induced approximately 20–25%, 15–20% and 7% shrinkage of vessel diameter respectively, relative to the null effect with normal saline. Similarly, CA4P and C118P showed no statistically significant difference in diameter effects.

Vessel density (*Figure 4C*) exhibited the greatest reduction at 35% by 10 mg C118P treatments, whereas CA4P at various concentrations induced 10–20% decreases. Both VDAs created statistically significant differences relative to the saline control. Higher concentration induced more density reduction. At control, densities at all intermediate time points are higher than the two terminal points, with a peak at 20 min, reflecting only a volume effect.

Vessel total length (*Figure 4D*) showed statistically significant reductions at doses of 10 and 5 mg/mL, with about 35% by C118P and 25% by CA4P respectively. Two VDAs at 2 mg/mL exerted the limited effects within 10%. Control treatment caused a similar trend as that with vascular density, implying a lack of VDAs' volume-counteractive effect.

Table 1 of statistical analyses demonstrates respectively the effects of three factors on four parameters (upper part) (36) and interactions between each two factors in details (lower part). Statistically significant differences (P<0.0001) are revealed among the three factors with respect to 4 parameters by multivariate ANOVA analyses.

Factor of treatment and parameter of blood perfusion are chosen as examples to explain here. A superscripted letter "a" appearing after the values with both CA4P and C118P in the table group means no statistically significant

Table 1 Multi-factorial analysis of variance analyses with interactions

Factors	Blood perfusion	Vascular diameter	Vascular density	Vascular length
Treatment				
CA4P	90.93±1.47[a]	97.73±0.99[a]	95.44±1.71[a]	96.63±1.87[a]
C118P	92.77±1.57[a]	99.70±1.39[a]	86.89±1.67[b]	84.56±1.53[b]
Saline	106.03±0.77[b]	107.27±0.89[b]	105.67±1.27[c]	107.67±1.79[c]
P value	<0.0001	<0.0001	<0.0001	<0.0001
Concentration, mg/mL				
10	90.59±1.77[a]	98.10±1.30[a]	90.06±1.99[a]	90.70±2.13[a]
5	96.24±1.36[b]	100.45±1.22[b]	94.38±1.82[b]	93.71±2.10[a]
2	102.89±0.91[c]	105.15±0.96[c]	101.19±1.47[c]	101.06±1.77[b]
Saline	106.09±1.06[d]	107.21±1.80[c]	105.67±2.38[d]	107.67±2.83[c]
P value	<0.0001	<0.0001	<0.0001	<0.0001
Time				
5 min	103.02±1.10[a]	106.69±0.90[a]	102.16±1.73[a]	102.48±2.29[a]
10 min	103.67±1.35[ab]	109.82±1.21[b]	100.48±1.85[ab]	102.97±2.66[a]
15 min	99.91±1.74[bc]	108.29±1.35[ab]	96.97±2.27[b]	96.26±1.99[b]
20 min	97.20±2.13[c]	99.69±1.35[c]	96.77±3.10[b]	96.16±3.03[b]
25 min	90.43±2.21[d]	93.43±1.48[d]	88.61±2.76[c]	88.48±3.31[c]
30 min	85.22±2.38[e]	89.47±1.55[e]	83.94±2.65[c]	82.29±2.68[d]
P value	<0.0001	<0.0001	<0.0001	<0.0001
Factor interactions (P values)				
Treatment × time	<0.0001	<0.0001	<0.0001	0.0894
Treatment × concentration	<0.0001	<0.0001	0.5679	1.0000
Concentration × time	0.0063	0.4729	0.7435	0.2011

Data are expressed as relative percentage values (mean ± standard error of the mean) after being standardized against the initial values. Three factors (treatment, concentration, time) as analytical variates are compared individually based on all possible pair combinations. Similar superscripted letters (a, b, c, d, e) after each value indicate no significant difference (P>0.05) while comparing pairs within the same group of parameter versus the factor in the table. P values indicate overall difference comparing individual factors or parameters.

difference in-between CA4P and C118P (P>0.05); whereas a superscripted letter "b" after the value with saline denotes its statistically significant difference (P<0.0001) against CA4P and C118P individually. Overall, P<0.0001 in this group demonstrates that two VDAs have significant impacts on CAM blood perfusion. All other P<0.0001 values in the upper part of *Table 1* express that the three factors have significant impacts on all four parameters. In the group Concentration and Time, different superscripted letters "a" "b" "c" "d" "e" demonstrate that the two paired values are of statistically significant difference from each other.

From the interactions between paired factors (lower part of *Table 1*), it is demonstrated that "treatment" and "time" interact significantly on blood perfusion, vascular diameter, vascular density, but not on vascular length; "treatment" and "concentration" interact significantly on blood perfusion, vascular diameter, but not on the other two parameters; "concentration" and "time" interact significantly on blood perfusion, but not on the other three parameters. Blood perfusion and vessel diameter are more sensitive to the factors than vessel density and length.
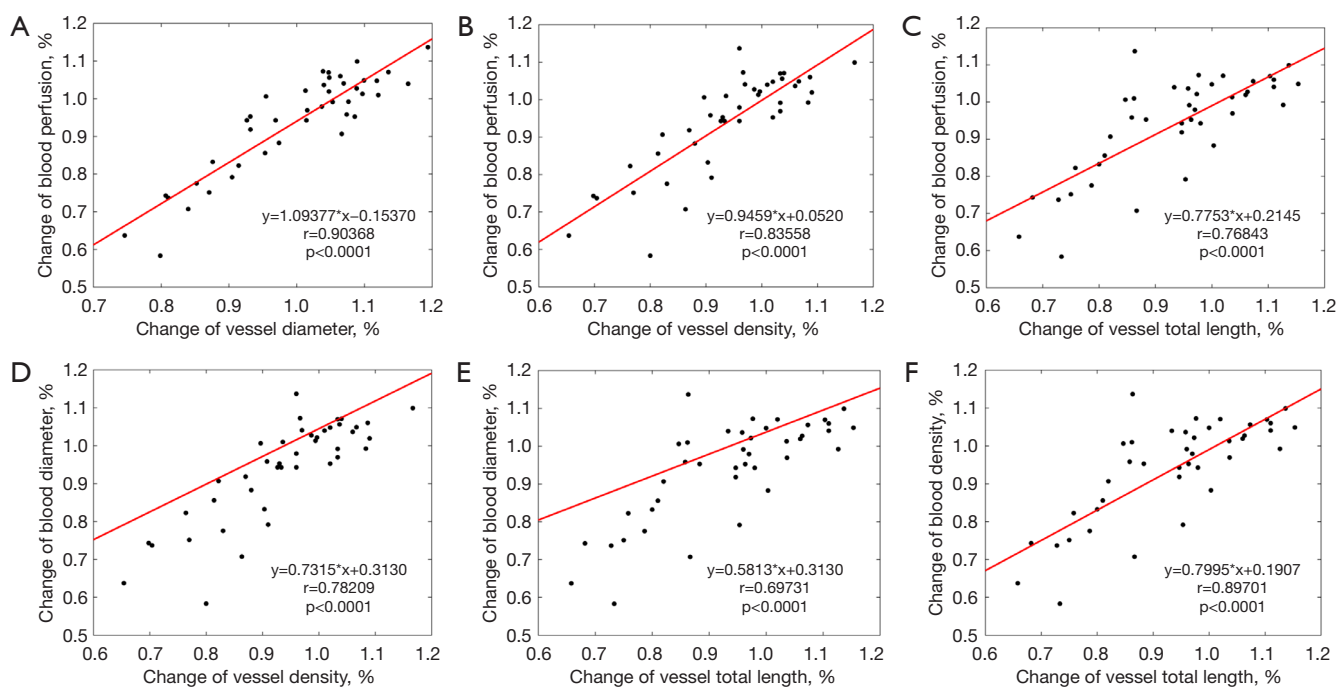
Figure 5 Linear regression analyses for the correlations between two parameters. (A) Blood perfusion-vessel diameter; (B) blood perfusion-vessels density; (C) blood perfusion-vessels total length; (D) vessel diameter-vessels density; (E) vessel diameter-vessels total length; (F) vessels density-vessels total length.

Cross correlations of multi-parameters

The correlations between each two parameters were also analyzed and shown in *Figure 5* to determine correct selection of parameters and potential mutual influences. Totally six pairs of correlation are listed, which all demonstrate positive-correlation profiles with statistical significance ($P<0.0001$). Each equation and r value are respectively given (*Figure 5*).

FIHC of cytoskeleton and insight on molecular mechanism

Qualitative observations

The effects of VDAs on the main components of cytoskeleton including β-tubulin and F-actin were evaluated to further explore the molecular mechanisms on vascular endothelial cells in response to VDAs.

As shown in *Figure 6*, green fluorescent β-tubulin networks are prominent in the saline control group, from endothelia to other peripheral structures. By contrast, green fluorescence diminished on images with both CA4P and C118P as a function of their incremental doses, suggesting depolymerized tubulin in cytoskeleton of endothelium by these two VDAs.

At 2 mg/mL concentration of them, green fluorescence from vascular endothelia is fairly visible. But, both VDAs at 5 mg/mL concentration result in a significantly faded green fluorescence of tubulin network. At concentration of 10 mg/mL, both CA4P and C118P cause virtually disappearance of green fluorescence and the vascular structure becomes almost undiscernible presumably due to a lack of tubulin network. Collectively, comparing FIHC images, C118P demonstrated more severe tubulin disruption on normal CAM vessels than CA4P at the same concentration levels.

Controversial to the suggested tubulin depolymerization, there is no disrupting effect of both VDAs on the F-actin component of the endothelial cytoskeleton. FIHC proves that different concentrations of VDAs did not affect the degrees of red fluorescence with F-actin and VDAs selectively disrupted only one component (tubulin) of endothelial cytoskeleton in normal blood vessels. VDAs does not seem to affect red blood cells either.

Quantitative measurements

Quantitative measurements and analyses of the mean fluorescent intensities for both β-tubulin and F-actin in terms of VDA treatments and concentrations are
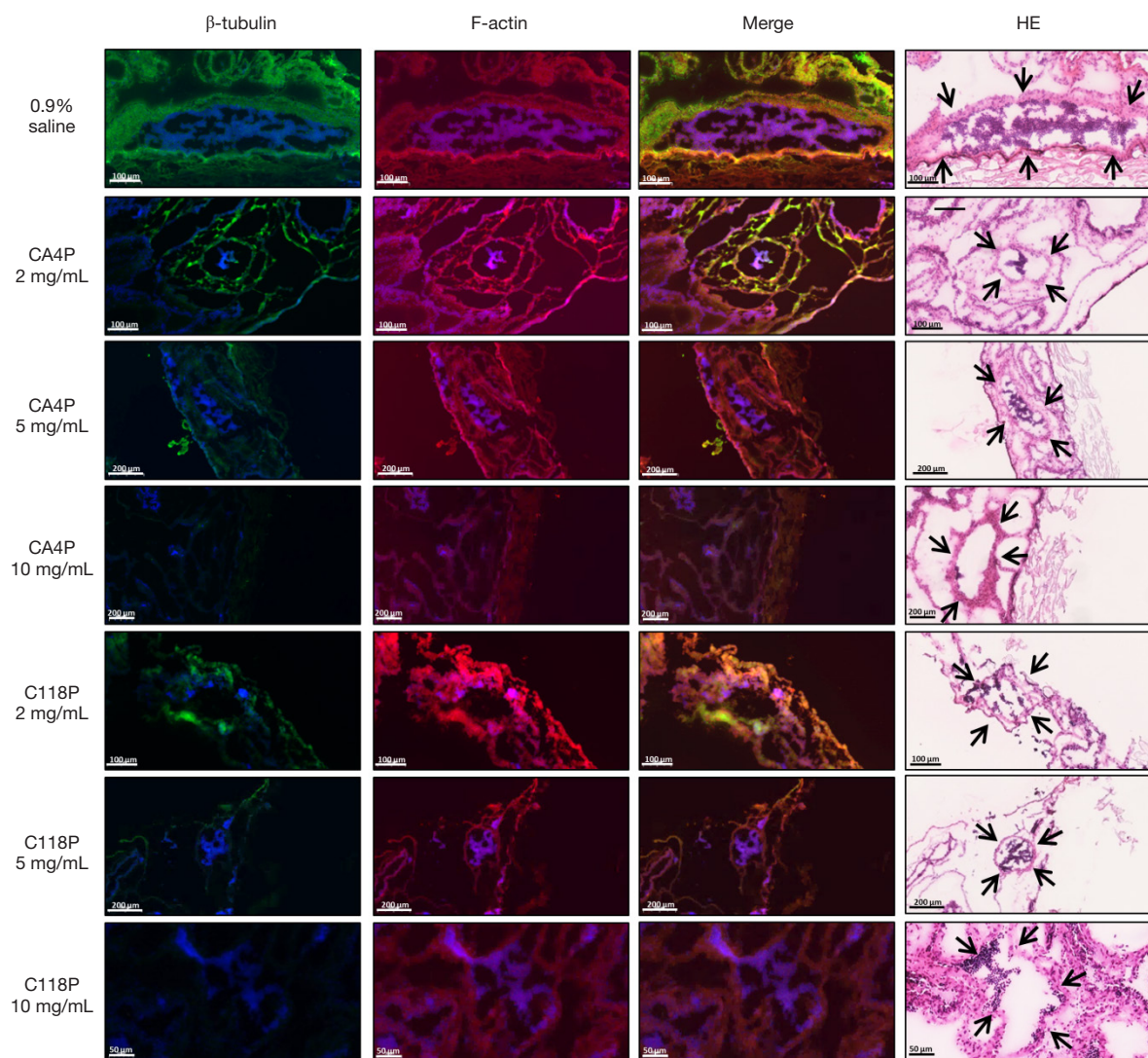
Figure 6 FIHC microscopies on vascular endothelial cytoskeleton in chorioallantoic membrane. Pictures of β-tubulin (green fluorescence) and F-actin (red fluorescence) and merged images are displayed against the treatment with 0.9% saline (control), CA4P (2, 5, 10 mg/mL) and C118P (2, 5, 10 mg/mL), respectively, to demonstrate cytoskeletal changes. Nuclei are counterstained with DAPI (blue). On HE stained slide, arrows indicate the focused blood vessels with endothelial cells. All magnifications are ×200. The nucleated chicken red blood cells are counterstained in blue color by DAPI (34), which facilitate visualizing vascular structures and contrasting with β-tubulin and F-actin. FIHC, fluorescent immunohistochemistry; CA4P, combretastatin A4-phosphate; DAPI, 4',6-diamidino-2-phenylindole; HE, hematoxylin-eosin.

summarized in *Tables 2,3* respectively with statistical results.

From *Table 2*, ANOVA analysis reveals statistically significant differences between saline control and two VDAs treatments on β-tubulin, but no difference in-between the two VDAs, suggesting ascertained effects of VDAs on β-tubulin cytoskeleton of normal CAM vessels.

In terms of concentrations, there is no difference between saline control and 2 mg/mL, but an increasingly significant difference between control and 5 and 10 mg/mL,

respectively; with no difference between 5 and 10 mg/mL, yet significant differences between 2 and 5 mg/mL or between 2 and 10 mg/mL.

From *Table 3*, ANOVA analysis reveals no difference at all between control and treatments with two VDAs on F-actin of cytoskeleton in normal CAM vasculature, in terms of both applied VADs and their concentrations relative to saline control.

The above CAM findings support the notions that

Table 2 β-tubulin fluorescent immunohistochemistry analysis of variance analysis

Factors	Mean fluorescent intensity		Multi-variates	
	Variates	Value	Pair combinations	P
Treatments	0.9% saline 0.5 mL	32.40±3.87	Control-CA4P	0.004
	CA4P	16.39±2.58	Control-C118P	0.006
	C118P	17.41±2.58	CA4P-C118P	0.784
Concentrations	0.9% saline	32.40±3.87	Control-2 mg/mL	0.603
	2 mg/mL	29.75±3.16	Control-5 mg/mL	0.002
	5 mg/mL	13.70±3.16	Control-10 mg/mL	0.000
	10 mg/mL	7.25±3.16	2 mg/mL-5 mg/mL	0.003
			2 mg/mL-10 mg/mL	0.000
			5 mg/mL-10 mg/mL	0.169

Mean fluorescent intensity values (mean ± standard error of the mean) were measured and presented for β-tubulin. Two factors (treatment, concentration) as analytical variates are distinguished individually based on all possible pair combinations. Significant difference was set at $P<0.05$.

Table 3 F-actin fluorescent immunohistochemistry analysis of variance analysis

Factors	Mean fluorescent intensity		Multi-variates	
	Variates	Value	Pair combinations	P
Treatments	0.9% saline 0.5 mL	54.60±12.33	Control-CA4P	0.523
	CA4P	44.90±8.22	Control-C118P	0.841
	C118P	57.63±8.22	CA4P-C118P	0.291
Concentrations	0.9% saline	54.60±12.33	Control-2 mg/mL	0.739
	2 mg/mL	60.00±10.07	Control-5 mg/mL	0.528
	5 mg/mL	44.33±10.07	Control-10 mg/mL	0.752
	10 mg/mL	49.49±10.07	2 mg/mL-5 mg/mL	0.288
			2 mg/mL-10 mg/mL	0.471
			5 mg/mL-10 mg/mL	0.723

Mean fluorescent intensity values (mean ± standard error of the mean) were measured and presented for F-actin. Two factors (treatment, concentration) as analytical variates are distinguished individually based on all possible pair combinations. Significant difference was set at $P<0.05$.

VDAs selectively affect tubulin alone and simultaneously keep F-actin intact, which is the basis of VDAs for their anticancer property (1-3).

Correlations of FIHC with LSCI derived parameters
FIHC molecular assay corresponded and verified the results of four LSCI derived functional and morphological parameters (*Figure* 7). Mean values of β-tubulin and F-actin fluorescent intensity are applied in correlation analysis.

In the upper row, all four pairs demonstrate positive-correlation profiles with statistical significance for β-tubulin. Contrarily in the lower row, all four pairs fail to show any correlation profiles with F-actin. Such correlation analyses have again verified the VDAs' specificity on tubulin.

Discussion

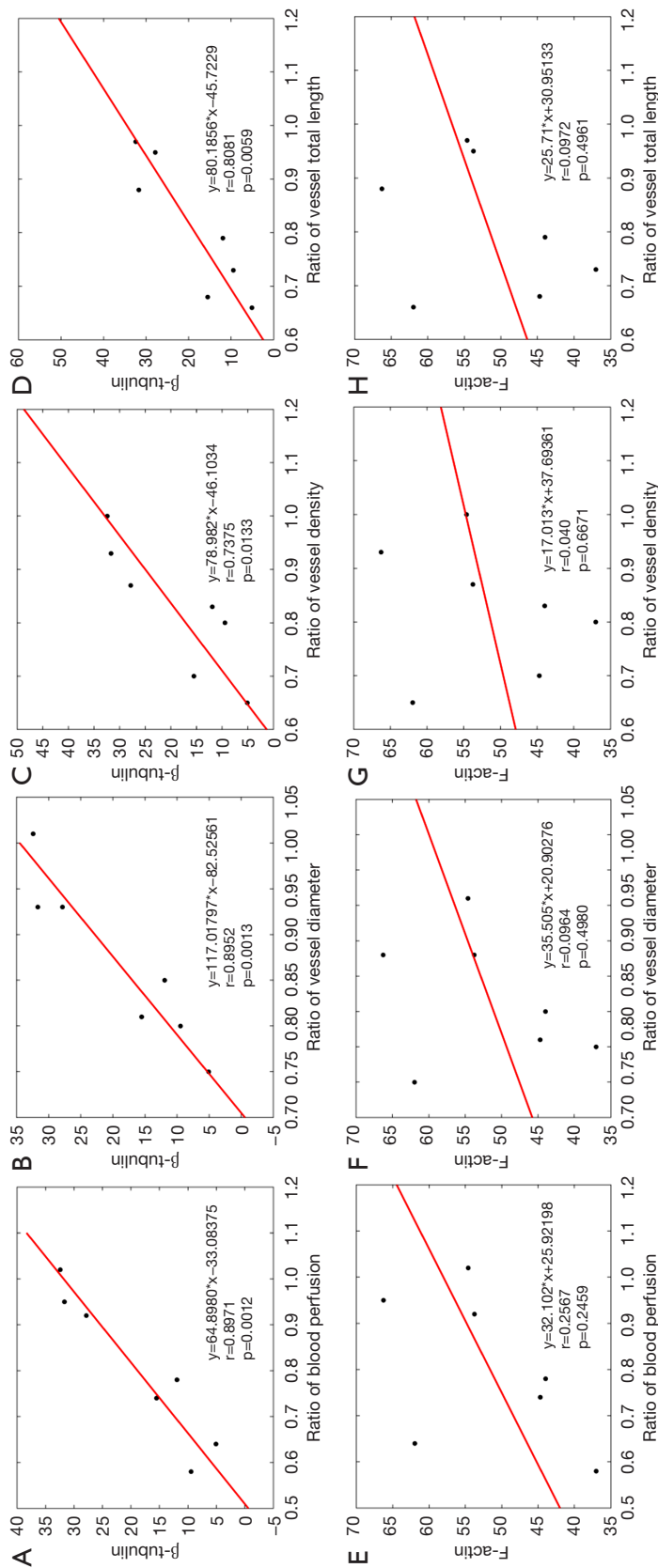Based on the present LSCI-CAM platform for evaluation

Figure 7 Linear regression analyses for the correlations between mean β-tubulin (upper row) and F-actin (lower row) fluorescent intensities against four LSCI derived parameters. (A) β-tubulin-blood perfusion; (B) β-tubulin-vessel diameter; (C) β-tubulin-vessel density; (D) β-tubulin-vessel total length; (E) F-actin-blood perfusion; (F) F-actin-vessel diameter; (G) F-actin-vessel intensity; (H) F-actin-vessel total length. Equation, R value and P value are respectively given. LSCI, laser speckle contrast imaging.

of vasoactive medications (26) at ED12 assisted with a deep learning setting, under constant intravascular infusion of two VDAs for 30 min, four parameters of blood perfusion, vessel diameter, vessel density and vessel total length have been collected and analyzed. Both qualitative observation and quantitative measurements on these four parameters have been successfully executed. The results comprehensively demonstrated the effects of two VDAs on CAM vasculature, supported by multi-factorial ANOVA analysis with statistical significance. The specific interactions among factors and correlations between parameters have been verified. Molecular FIHC assays of cytoskeleton performed in this study have yielded more insights on the mechanism underlying VDAs' pharmacologic effects. This combination of platforms proves innovative for *in vivo* evaluations of vascular-targeting drugs, particularly in compliance with current 3R principle in scientific experimental research. To the best of our knowledge and of literature review, it is the first time that VDAs have been comprehensively evaluated *in vivo* in the CAM of chick embryos by using LSCI for multiparametric hemodynamic assessment and FIHC for molecular verifications, suggesting a new methodology for preclinical screening of tubulin and actin cytoskeleton interfering drugs. The clinicians may refer our discoveries to execute more precautions when VDAs eventually entering clinical applications. Those results might systemically extend to and inform next studies with tumour models and other vasoactive medications.

Cooperation of LSCI-CAM platform and IKOSA deep learning model

LSCI-CAM platform could efficiently and effectively monitor the hemodynamic alterations in real-time, in which blood perfusion is a major functional parameter to study vasculature in ovo. However, in view of the frontier deep learning technology to assist bio-medical research, IKOSA deep learning platform was integrated to introduce new morphological parameters in this study. Normally the deep learning model requires microscopic CAM images for the analysis, and LSCI-CAM platform could just generate colorful Flux images. Whereas in a recent study, LSCI and IKOSA deep learning platform were designed and established as two independent methods for angiogenesis measurement (37).

However, we explored to integrate two platforms in current research, Flux images were converted into grayscale images and put into IKOSA platform for analysis, which proved feasible. Through measurement and statistical analysis, it has confirmed that more accurate results and factorial interactions could be created through LSCI-CAM platform.

Performance of two VDAs

Tubulin-binding agents of small molecular VDAs are selected as medications in current study, because this class of drugs are currently under intensive research. CA4P is the first VDA discovered and has advanced to phase 3 clinical trials (38). C118P is newly synthesized VDA, with improved water solubility and prolonged half-life, and has been tested in preclinical pharmacokinetics (39) and pharmacological (40) studies as well as in early clinical trials. Based on blood perfusion and vascular diameter, two VDAs exerted the same effects on normal vessels without statistically significant difference. However, on vascular density and total vascular length, C118P showed significantly stronger effects on morphology of normal vasculature than CA4P, of which clinical influence has to be investigated.

Correlation between blood perfusion and vascular diameter

In a previous publication (26), a reverse correlation between blood perfusion and vascular diameter was documented during the vascular evolution of chick embryos from ED9 to ED12. However in current research, a positive correlation between blood perfusion and vascular diameter was uncovered. However, unlike the observations on the natural vascular evolution during ED 9 and ED 15 in the previous study (26), it must be noted that the current study monitored vascular alterations during 30 min under the treatment of VDAs on ED 12, which involved the pharmacological effects of vasoactive drugs.

Volumetric effects

Most obviously seen in saline control group, all of four parameters experienced a parabolic trend phenomenon during 30 min intravascular infusion, which could be related to volumetric effects caused by slow infusion of 0.5 mL saline solution into the enclosed vascular circulation of the embryonic egg with a total blood volume about 2.0 ml on ED 12 (41). Those blood and vascular parameters returned to normal levels probably due to physiological adaptation by the embryo to excrete the extra normal saline into urine. However, in the VDA treatment groups, although the same

phenomenon of less extents could also be observed, the values of all parameters declined with later time due to the VDAs' pharmacological effects that counteracted to the volumetric effects in a dose dependent manner.

Clinical implications

This experiment explored both gross vascular alterations and molecular mechanisms after the treatment with both VDAs, which might be referential to their clinical applications. Based on our results, these VDAs transiently disrupted the overall normal vasculature to a certain extent, which is somewhat different from the previous notions about tumor selectivity of VDAs (2,3,6,7). For instance, the narrowed diameter of normal blood vessels (*Figure 4B*) caused by VDAs' effect could explain the transient hypertension as an adverse effect observed during drug infusion in patients of clinical trials (38), to whom proper antihypertensive drugs should be made ready to prevent severe therapy-related complications.

Study limitations

There existed some technical limitations in this study. For example, when Flux images were converted into grayscale images for IKOSA platform processing and analysis, imaging artifacts may appear, which were mainly caused by wrinkles of CAM, contrast fluctuation, light reflection, depth of vessels, etc. In the future, it is necessary to de-noise images before proceeding with the deep learning platform by additional algorithms and noise filters (42-44).

Regarding FIHC assays, CD31 and CD34 are endothelium-specific biomarkers to characterize and illustrate the structures and alterations of blood vessels. However, we failed to obtain fluorescence-tagged antibodies particularly for chick origin and to realize in this research, which remained a pity that however was fortunately overcome by the acquisitions of dedicated β-tubulin and F-actin FIHC kits as demonstrated in this paper (*Figure 6*).

Conclusions

LSCI-CAM platform in combination with a deep learning platform was proved effective to execute preclinical evaluations of two VDAs on normal vasculature of CAM. The four parameters (blood perfusion, vessel diameter, vessel density and vessel total length) characterizing normal vasculature could be positively correlated to each other, and

negatively affected by applied VDAs in a dose dependent manner with statistical significance. Such findings could explain the phenomena of side-effects on patients in clinical trials. FIHC assay of endothelial cytoskeleton by β-tubulin and F-actin could verify these discoveries at molecular levels.

Footnote

Conflicts of Interest: All authors have completed the ICMJE uniform disclosure form (available at https://qims.amegroups.com/article/view/10.21037/qims-23-1065/coif). Y.N. serves as an unpaid editorial board member of *Quantitative Imaging in Medicine and Surgery*. The other authors have no conflicts of interest to declare.

Ethical Statement: The authors are accountable for all aspects of the work in ensuring that questions related to the accuracy or integrity of any part of the work are appropriately investigated and resolved. Ethical approval was waived by the Institutional Ethics Committee of KU Leuven since chick embryos are not considered animals before ED18, in compliance with The European Parliament and the European Council Directive 2010/63/EU.

Open Access Statement: This is an Open Access article distributed in accordance with the Creative Commons Attribution-NonCommercial-NoDerivs 4.0 International License (CC BY-NC-ND 4.0), which permits the non-commercial replication and distribution of the article with the strict proviso that no changes or edits are made and the original work is properly cited (including links to both the formal publication through the relevant DOI and the license). See: https://creativecommons.org/licenses/by-nc-nd/4.0/.

References

1. Liu Y, Wang S, Zhao X, Feng Y, Bormans G, Swinnen J, Oyen R, Huang G, Ni Y, Li Y. Predicting Clinical Efficacy of Vascular Disrupting Agents in Rodent Models of Primary and Secondary Liver Cancers: An Overview with Imaging-Histopathology Correlation. Diagnostics (Basel) 2020;10:78.

2. Siemann DW. The unique characteristics of tumor vasculature and preclinical evidence for its selective disruption by Tumor-Vascular Disrupting Agents. Cancer Treat Rev 2011;37:63-74.

3. Chase DM, Chaplin DJ, Monk BJ. The development and use of vascular targeted therapy in ovarian cancer. Gynecol Oncol 2017;145:393-406.

4. Chen L, Wang S, Feng Y, Zhang J, Du Y, Zhang J, Ongeval CV, Ni Y, Li Y. Utilisation of Chick Embryo Chorioallantoic Membrane as a Model Platform for Imaging-Navigated Biomedical Research. Cells 2021;10:463.

5. Cooney MM, van Heeckeren W, Bhakta S, Ortiz J, Remick SC. Drug insight: vascular disrupting agents and angiogenesis--novel approaches for drug delivery. Nat Clin Pract Oncol 2006;3:682-92.

6. Hinnen P, Eskens FA. Vascular disrupting agents in clinical development. Br J Cancer 2007;96:1159-65.

7. Wang S, Liu Y, Feng Y, Zhang J, Swinnen J, Li Y, Ni Y. A Review on Curability of Cancers: More Efforts for Novel Therapeutic Options Are Needed. Cancers (Basel) 2019;11:1782.

8. Garon EB, Neidhart JD, Gabrail NY, de Oliveira MR, Balkissoon J, Kabbinavar F. A randomized Phase II trial of the tumor vascular disrupting agent CA4P (fosbretabulin tromethamine) with carboplatin, paclitaxel, and bevacizumab in advanced nonsquamous non-small-cell lung cancer. Onco Targets Ther 2016;9:7275-83.

9. Sosa JA, Elisei R, Jarzab B, Balkissoon J, Lu SP, Bal C, Marur S, Gramza A, Yosef RB, Gitlitz B, Haugen BR, Ondrey F, Lu C, Karandikar SM, Khuri F, Licitra L, Remick SC. Randomized safety and efficacy study of fosbretabulin with paclitaxel/carboplatin against anaplastic thyroid carcinoma. Thyroid 2014;24:232-40.

10. Zweifel M, Jayson GC, Reed NS, Osborne R, Hassan B, Ledermann J, Shreeves G, Poupard L, Lu SP, Balkissoon J, Chaplin DJ, Rustin GJS. Phase II trial of combretastatin A4 phosphate, carboplatin, and paclitaxel in patients with platinum-resistant ovarian cancer. Ann Oncol 2011;22:2036-41.

11. Siemann DW, Shi W. Dual targeting of tumor vasculature: combining Avastin and vascular disrupting agents (CA4P or OXi4503). Anticancer Res 2008;28:2027-31.

12. Kendrew J, Odedra R, Logié A, Taylor PJ, Pearsall S, Ogilvie DJ, Wedge SR, Jürgensmeier JM. Anti-tumour and anti-vascular effects of cediranib (AZD2171) alone and in combination with other anti-tumour therapies. Cancer Chemother Pharmacol 2013;71:1021-32.

13. Monk B, Alvarez R, Chan J, Chase D, Herzog T, Couchenour R, et al. FOCUS study: physician's choice chemotherapy (PCC) plus bevacizumab and CA4P versus PCC plus bevacizumab and placebo in platinum-resistant ovarian cancer. International Gynecologic Cancer Societ; Lisbon, Portugal 2016.

14. Ciric E, Sersa G. Radiotherapy in combination with vascular-targeted therapies. Radiol Oncol 2010;44:67-78.

15. Ni Y. Abstract 1767: Oncocidia: a small molecule dual targeting pan-anticancer theragnostic strategy. Cancer Res 2014;74:1767.

16. Hasani A, Leighl N. Classification and toxicities of vascular disrupting agents. Clin Lung Cancer 2011;12:18-25.

17. Subbiah IM, Lenihan DJ, Tsimberidou AM. Cardiovascular toxicity profiles of vascular-disrupting agents. Oncologist 2011;16:1120-30.

18. Griggs J, Hesketh R, Smith GA, Brindle KM, Metcalfe JC, Thomas GA, Williams ED. Combretastatin-A4 disrupts neovascular development in non-neoplastic tissue. Br J Cancer 2001;84:832-5.

19. Shahrivari M, Wise E, Pettiford LC, Chaplin DJ, Pepine CJ, Cogle CR. Abstract P112: Mechanism of the Blood Pressure Response to a Novel Vascular Disrupting Combretastatin A1-Diphosphate (OXi4503). Hypertension 2015;66:AP112.

20. Victorelli FD, Cardoso VMO, Ferreira NN, Calixto GMF, Fontana CR, Baltazar F, Gremião MPD, Chorilli M. Chick embryo chorioallantoic membrane as a suitable in vivo model to evaluate drug delivery systems for cancer treatment: A review. Eur J Pharm Biopharm 2020;153:273-84.

21. Su M, Huang J, Liu S, Xiao Y, Qin X, Liu J, Pi C, Luo T, Li J, Chen X, Luo Z. The anti-angiogenic effect and novel mechanisms of action of Combretastatin A-4. Sci Rep 2016;6:28139.

22. Ribatti D. The chick embryo chorioallantoic membrane as a model for tumor biology. Exp Cell Res 2014;328:314-24.

23. Burggren W, Rojas Antich M. Angiogenesis in the Avian Embryo Chorioallantoic Membrane: A Perspective on Research Trends and a Case Study on Toxicant Vascular Effects. J Cardiovasc Dev Dis 2020;7:56.

24. Schneider-Stock R, Ribatti D. The CAM Assay as an Alternative In Vivo Model for Drug Testing. Handb Exp Pharmacol 2021;265:303-23.

25. Kunze P, Kreiss L, Novosadová V, Roehe AV, Steinmann S, Prochazka J, Geppert CI, Hartmann A, Schürmann S, Friedrich O, Schneider-Stock R. Multiphoton Microscopy Reveals DAPK1-Dependent Extracellular Matrix Remodeling in a Chorioallantoic Membrane (CAM) Model. Cancers (Basel) 2022;14:2364.

26. Chen L, Wang S, Feng Y, Yu J, Coudyzer W, Van Ongeval C, Geng L, Li Y, Ni Y. Development and characterization of a chick embryo chorioallantoic membrane (CAM) based platform for evaluation of vasoactive medications. Microvasc Res 2022;142:104372.

27. The European Parliament. European Directive on the protection of animals used for scientific purposes 2010/63/EU. Brussels: The European Parliament; 2010.

28. Kauffmann P, Troeltzsch M, Cordesmeyer R, Heidekrueger PI, Schliephake H, Canis M, Wolff HA, Rave-Fraenk M, Stroebel P, Kehrer A, Prantl L, Aung T. Presentation of a variation of the chorioallantoic membrane set up as a potential model for individual therapy for squamous cell carcinoma of the oropharynx. Clin Hemorheol Microcirc 2017;67:453-7.

29. Nebritova O. A study of hemodynamics and the structure of capillary blood flow using the method of laser speckle contrast analysis LASCA. Journal of Physics Conference Series 2019;1348:012065.

30. Pion E, Asam C, Feder AL, Felthaus O, Heidekrueger PI, Prantl L, Haerteis S, Aung T. Laser speckle contrast analysis (LASCA) technology for the semiquantitative measurement of angiogenesis in in-ovo-tumor-model. Microvasc Res 2021;133:104072.

31. Bamps D, Macours L, Buntinx L, de Hoon J. Laser speckle contrast imaging, the future DBF imaging technique for TRP target engagement biomarker assays. Microvasc Res 2020;129:103965.

32. van As K, Boterman J, Kleijn CR, Kenjeres S, Bhattacharya N. Laser speckle imaging of flowing blood: A numerical study. Phys Rev E 2019;100:033317.

33. Padmanaban P, Chizari A, Knop T, Zhang J, Trikalitis VD, Koopman B, Steenbergen W, Rouwkema J. Assessment of flow within developing chicken vasculature and biofabricated vascularized tissues using multimodal imaging techniques. Sci Rep 2021;11:18251.

34. Dark GG, Hill SA, Prise VE, Tozer GM, Pettit GR, Chaplin DJ. Combretastatin A-4, an agent that displays potent and selective toxicity toward tumor vasculature. Cancer Res 1997;57:1829-34.

35. BARNES AE, JENSEN WN. Blood volume and red cell concentration in the normal chick embryo. Am J Physiol 1959;197:403-5.

36. Samaee SM, Patzner RA, Mansour N. Morphological differentiation within the population of Siah Mahi,Capoeta capoeta gracilis, (Cyprinidae, Teleostei) in a river of the south Caspian Sea basin: a pilot study. Journal of Applied Ichthyology 2009;25:583-90.

37. Kuri PM, Pion E, Mahl L, Kainz P, Schwarz S, Brochhausen C, Aung T, Haerteis S. Deep Learning-Based Image Analysis for the Quantification of Tumor-Induced Angiogenesis in the 3D In Vivo Tumor Model-Establishment and Addition to Laser Speckle Contrast Imaging (LSCI). Cells 2022;11:2321.

38. Grisham R, Ky B, Tewari KS, Chaplin DJ, Walker J. Clinical trial experience with CA4P anticancer therapy: focus on efficacy, cardiovascular adverse events, and hypertension management. Gynecol Oncol Res Pract 2018;5:1.

39. Zhang C, Zhang X, Wang G, Peng Y, Zhang X, Wu H, Yu B, Sun J. Preclinical Pharmacokinetics of C118P, a Novel Prodrug of Microtubules Inhibitor and Its Metabolite C118 in Mice, Rats, and Dogs. Molecules 2018;23:2883.

40. Yang M, Su Y, Wang Z, Du D, Wei S, Liao Z, Zhang Q, Zhao L, Zhang X, Han L, Jiang J, Zhan M, Sun L, Yuan S, Zhou Z. C118P, a novel microtubule inhibitor with anti-angiogenic and vascular disrupting activities, exerts anti-tumor effects against hepatocellular carcinoma. Biochem Pharmacol 2021;190:114641.

41. Rychter Z, Kopecky M, Lemez L. A micromethod for determination of the circulating blood volume in chick embryos. Nature 1955;175:1126-7.

42. Sharma T. Various Types of Image Noise and De-noising Algorithm. International Journal of Modern Education and Computer Science 2017;9:50-8.

43. Liu S, Rahman MA, Liu SC, Yeow Wong C, Lin CF, Wu H, Kwok N. Image de-hazing from the perspective of noise filtering. Computers & Electrical Engineering 2017;62:345-59.

44. Lu J, Yang Z, Shen L, Lu Z, Yang H, Xu C. A framelet algorithm for de-blurring images corrupted by multiplicative noise. Applied Mathematical Modelling 2018;62:51-61.